

Novel Strongly Spin-Orbit Coupled Quantum Dimer Magnet: $\text{Yb}_2\text{Si}_2\text{O}_7$ Gavin Hester,^{1,*} H. S. Nair,¹ T. Reeder,¹ D. R. Yahne,¹ T. N. DeLazzer,¹ L. Berges,² D. Ziat,² J. R. Neilson,³
A. A. Aczel,⁴ G. Sala,⁴ J. A. Quilliam,^{2,†} and K. A. Ross^{1,5,‡}¹*Department of Physics, Colorado State University, 200 W. Lake St., Fort Collins, Colorado 80523-1875, USA*²*Institut Quantique and Département de Physique, Université de Sherbrooke,
2500 boulevard de l'Université, Sherbrooke, Québec J1K 2R1, Canada*³*Department of Chemistry, Colorado State University, 200 W. Lake St., Fort Collins, Colorado 80523-1872, USA*⁴*Neutron Scattering Division, Oak Ridge National Laboratory, Oak Ridge, Tennessee 37831, USA*⁵*Quantum Materials Program, Canadian Institute for Advanced Research (CIFAR), Toronto, Ontario M5G 1Z8, Canada*

(Received 31 October 2018; published 9 July 2019)

The quantum dimer magnet (QDM) is the canonical example of quantum magnetism. The QDM state consists of entangled nearest-neighbor spin dimers and often exhibits a field-induced triplon Bose-Einstein condensate (BEC) phase. We report on a new QDM in the strongly spin-orbit coupled, distorted honeycomb-lattice material $\text{Yb}_2\text{Si}_2\text{O}_7$. Our single crystal neutron scattering, specific heat, and ultrasound velocity measurements reveal a gapped singlet ground state at zero field with sharp, dispersive excitations. We find a field-induced magnetically ordered phase reminiscent of a BEC phase, with exceptionally low critical fields of $H_{c1} \sim 0.4$ and $H_{c2} \sim 1.4$ T. Using inelastic neutron scattering in an applied magnetic field we observe a Goldstone mode (gapless to within $\delta E = 0.037$ meV) that persists throughout the entire field-induced magnetically ordered phase, suggestive of the spontaneous breaking of U(1) symmetry expected for a triplon BEC. However, in contrast to other well-known cases of this phase, the high-field ($\mu_0 H \geq 1.2$ T) part of the phase diagram in $\text{Yb}_2\text{Si}_2\text{O}_7$ is interrupted by an unusual regime signaled by a change in the field dependence of the ultrasound velocity and magnetization, as well as the disappearance of a sharp anomaly in the specific heat. These measurements raise the question of how anisotropy in strongly spin-orbit coupled materials modifies the field induced phases of QDMs.

DOI: [10.1103/PhysRevLett.123.027201](https://doi.org/10.1103/PhysRevLett.123.027201)

Quantum dimer magnets (QDMs) represent the simplest case of quantum magnetism, where entanglement is a required ingredient for even a qualitative understanding of the phase. In a QDM, entangled pairs of spins form $S_{\text{tot}} = 0$ dimers and result in a nonmagnetic ground state. The excited states of these entangled spins can be treated as bosons, called triplons, which can undergo Bose-Einstein condensation (BEC) as their density is tuned by an applied magnetic field. This BEC state is a magnetic field-induced long range ordered phase, which occupies a symmetric “dome” in the field vs temperature phase diagram with two temperature-dependent critical fields, $H_{c1}(T)$ and $H_{c2}(T)$. The vast majority of the previously studied QDMs are based on $3d$ transition metal ions with “bare” (spin-only) $S = 1/2$ or $S = 1$ angular momentum, resulting in simple Heisenberg or XXZ spin interaction Hamiltonians, and high critical fields set by the relatively high energy scale of exchange interactions [1–6].

Lanthanide-based magnetic materials with spin-orbit coupled pseudospin $1/2$ ($S_{\text{eff}} = 1/2$) angular momenta can also exhibit quantum phases, and these are often directly analogous to their traditional $3d$ transition metal ion counterparts. However, entirely new phases are possible due to the anisotropic exchange in these materials [7–12].

In the lanthanide series, Yb^{3+} has been of particular interest as it can generically host interactions leading to quantum fluctuations irrespective of the crystal electric field (CEF) ground state doublet composition [13]. Indeed, various quantum phases have been discovered in Yb-based systems [14–20]. However, a notable absence in the growing lineup of Yb quantum materials is a material exhibiting a QDM with a field-induced BEC state. The opportunity to study such a material could lead to the observation of new phases describable by theories of interacting bosons, as well as new types of quantum phase transitions.

As a previously studied example, the metallic material YbAl_3C_3 was shown to host Yb dimerization and triplet excitations [21,22]. However, an unusual field-induced ordered state was observed whose onset temperature far exceeds the spin gap energy [23], suggesting that it is not directly related to the singlet-triplet excitation (unlike a field-induced BEC phase). Additionally, YbAl_3C_3 shows field-induced *disordered* regimes that have yet to be fully understood, particularly in the context of the additional Kondo and RKKY interactions involving the conduction electrons in this material [24–26]. This material demonstrates that quantum dimerization is possible in lanthanide-based magnetic materials, but does not always lead to a

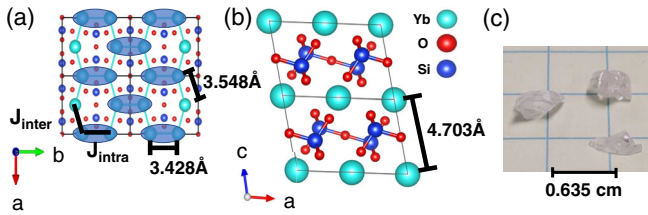


FIG. 1. (a) Crystal structure of $\text{Yb}_2\text{Si}_2\text{O}_7$ viewed along the c axis, where Yb atoms are light green and form a distorted honeycomb lattice, Si atoms are blue, and O atoms are red [27]. Intradimer and interdimer bond lengths are shown (3% anisotropy), and J_{intra} and J_{inter} exchange tensors are labeled. The blue ovals indicate the probable location of the dimers. (b) Crystal structure viewed along the b axis, showing the separation of the layers of Yb honeycombs. (c) Characteristic crystals obtained from breaking the crystal boule. The crystals are clear and colorless.

field-induced BEC phase. Naively, one might not expect a highly spin-orbit coupled material to exhibit BEC, which requires the exchange Hamiltonian to be at least $U(1)$ symmetric (i.e., XXZ type interactions). Although recent work has demonstrated that for ideal, edge-sharing octahedral environments, Heisenberg exchange is indeed expected to dominate in Yb materials [13], such high exchange symmetry is not *a priori* expected for nonideal local environments. However, a recent example of high exchange symmetry for Yb^{3+} in a nonideal crystal field environment has been discovered in the Tomonaga-Luttinger liquid YbAlO_3 [16], suggesting that it may be more common than expected. Yet even with dominant Heisenberg interactions, smaller anisotropic terms should still be relevant which, in the case of a QDM, would be expected to modify the field-induced phases. Furthermore, Yb-based QDMs should provide a convenient testing ground for field-induced BEC physics due to reduced exchange energy compared to materials based on $3d$ transition metals. This leads to lower critical fields, which can be accessed by continuous field magnets, thus enabling experimental techniques such as inelastic neutron scattering (INS) to be brought to bear on the full phase diagram. This is the case for $\text{Yb}_2\text{Si}_2\text{O}_7$, as we show here.

$\text{Yb}_2\text{Si}_2\text{O}_7$ [monoclinic space group $C2/m$, room temperature lattice parameters of $a = 6.7714(9)$ Å, $b = 8.8394(2)$ Å, $c = 4.6896(5)$ Å, $\beta = 101.984(9)^\circ$ [28]] was previously studied in the context of polymorphism in the $\text{RE}_2\text{Si}_2\text{O}_7$ (rare-earth pyrosilicate) series [36,37], but its magnetic properties have not been reported. $\text{Yb}_2\text{Si}_2\text{O}_7$ has only one reported polymorph, known as the C-type pyrosilicate (Fig. 1). The single crystal samples of $\text{Yb}_2\text{Si}_2\text{O}_7$ used in this study were grown via the optical floating zone method [28,38]. Our growths have resulted in clear, colorless multicrystal boules which are then broken into smaller single crystal pieces as shown in Fig. 1(c).

Magnetization was measured using a MPMS XL Quantum Design SQUID magnetometer at $T = 1.8$ K along the a^* , b , and c directions. Field- and temperature-dependent specific heat was measured down to 50 mK using the quasiadiabatic heat pulse method in a Quantum Design Dynacool PPMS with a dilution refrigerator insert at Colorado State University, as well as a home-built dilution refrigerator at Université de Sherbrooke. $\text{Lu}_2\text{Si}_2\text{O}_7$ was also measured as a nonmagnetic analog. Ultrasound velocity experiments were performed down to 50 mK using a pulsed, time-of-flight interferometer. 30 MHz transducers were glued to parallel surfaces so as to propagate longitudinally polarized sound waves along the c^* axis. The absolute velocity of the quasilongitudinal mode studied here was approximately 3000 m/s and relative changes in velocity ($\Delta v/v$) were measured with high precision using a phase-lock loop. Powder neutron diffraction data were collected on BT1 at the NIST Center for Neutron Research with incident wavelength $\lambda = 2.0787$ Å and 60 arc min collimation. Synchrotron x-ray diffraction (SXR) data were recorded at $T = 295$ K at beam line 11 BM ($\lambda = 0.41418$ Å) at the Advanced Photon Source, Argonne National Laboratory. Time-of-flight INS experiments were performed at the Cold Neutron Chopper Spectrometer (CNCS) at the Spallation Neutron Source, Oak Ridge National Laboratory (ORNL). These INS data were collected using $E_i = 1.55$ meV neutrons in the “high flux” chopper setting mode, producing an energy resolution of $\delta E = 0.037$ meV at the elastic line [39], and were analyzed using the DAVE software package [40]. A neutron diffraction measurement using $E_i = 14.7$ meV neutrons was performed using the Fixed-Incident Energy Triple-Axis Spectrometer (FIE-TAX) on the HB-1A beam line at the High Flux Isotope Reactor at Oak Ridge National Laboratory, using collimator settings of 40° - 40° - 40° - 80° .

Rietveld analysis of the SXR data [28] confirms the previously reported crystal structure. Analysis of the zero field, high-temperature, magnetic specific heat of $\text{Yb}_2\text{Si}_2\text{O}_7$ confirms that a low energy $S_{\text{eff}} = 1/2$ picture applies at temperatures well below ~ 100 K [28]. The saturation magnetization at $T = 1.8$ K along three crystal directions gives the approximate g -values of $g_{a^*} = 3.2$, $g_b = 2.0$, and $g_c = 4.8$.

The zero-field specific heat shown in Fig. 2(a) displays a broad feature peaked at ~ 1 K, which can be fit to a dispersive four level Schottky anomaly form, consistent with an interacting spin dimer ground state. We used an approximation of an interacting triplon model to fit the zero-field specific heat [28], enforcing Heisenberg interactions. The fit yielded the parameters $J_{\text{intra}} = 0.236(4)$ meV and $J_{\text{inter}} = 0.06(2)$ meV. These parameters are similar to those extracted from fitting the field polarized spin wave spectrum: $J_{\text{intra}} = 0.217(3)$ and $J_{\text{inter}} = 0.089(1)$ meV [28]. The adequacy of Heisenberg interactions for reproducing both the zero field C_p and field-polarized INS data measurements suggests that $\text{Yb}_2\text{Si}_2\text{O}_7$ is another case in which

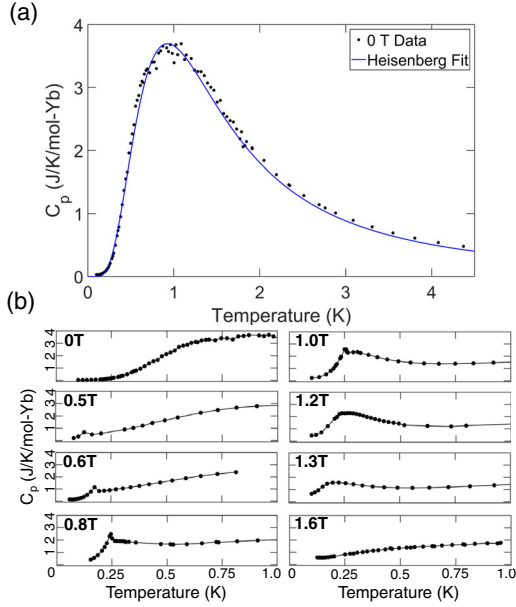


FIG. 2. (a) Zero-field specific heat and fit to a dispersive 4-level Schottky anomaly, using Heisenberg exchange for inter- and intradimer interactions [$J_{\text{intra}} = 0.236(4)$ meV, $J_{\text{inter}} = 0.06(2)$ meV]. (b) Specific heat of $\text{Yb}_2\text{Si}_2\text{O}_7$ at increasing fields with $H||c$. A sharp anomaly is visible at 0.5 T ($>H_{c1}$), which corresponds to a field-induced magnetically ordered state. The transition temperature maps out a dome as a function of field, but the sharp anomaly is replaced by a broad anomaly above ~ 1.2 T (H_m), which moves to lower temperatures with increasing field. Above H_{c2} (1.4 T), the broad anomaly shifts to higher temperatures with increasing field, consistent with field polarized paramagnetism.

Yb^{3+} interactions are unexpectedly predominantly isotropic. The entropy change through this low temperature Schottky anomaly (0.05 to 2 K), reaches the expected $R \ln 2$ per Yb [28], indicating that $\text{Yb}_2\text{Si}_2\text{O}_7$ does not undergo a magnetic

ordering transition at lower temperatures, and thus remains quantum disordered down to $T = 0$ K. This is further confirmed by the lack of magnetic Bragg peaks at 50 mK, as determined by both single crystal [Fig. 3(c)] and powder neutron diffraction measurements [28].

The field dependence ($H||c$) of the specific heat is shown in Fig. 2(b). At $H = 0.5$ T, a sharp anomaly appears at $T = 0.13$ K, which we have confirmed by neutron scattering to coincide with a transition to long range magnetic order via the appearance of magnetic Bragg peaks. With increasing field, the transition temperature maps out a dome in the H vs T phase diagram as expected for a BEC phase. As the field is increased further (0.8 T), a broad feature emerges, which eventually becomes the dominant feature above $H_m = 1.2$ T. The maximum of this broad feature then continues to trace out the high field region of the dome, with the temperature of the maximum decreasing with increasing field. At 1.6 T, the maximum of the broad feature is again increasing in temperature with increasing field as expected for a field-polarized paramagnetic regime.

Isothermal field scans of variations in sound velocity are shown in Fig. 3(a) for various temperatures. At the lowest temperatures ($T = 50$ mK) the sound velocity is largely field independent until $H_{c1} \simeq 0.4$ T, where $\Delta v/v$ begins decreasing with field. At $H_{c2} \simeq 1.4$ T, $\Delta v(H)$ reaches a minimum, before returning sharply to roughly the zero field value in the field polarized limit. In addition to the two expected critical fields, H_{c1} and H_{c2} , the sound velocity also exhibits a significant change in slope at roughly $H_m = 1.2$ T, suggesting the presence of an additional phase, as indicated in Fig. 3(b). Aside from the sharp change of slope at H_m , our sound velocity measurements resemble those performed on another quantum dimer magnet, $\text{Sr}_3\text{Cr}_2\text{O}_8$ [41]. In contrast, sound velocity measurements on $\text{NiCl}_2\text{-}4\text{SC}(\text{NH}_2)_2$ (also known as DTN) [42] show sharper dips at both H_{c1} and H_{c2} , which are attributed

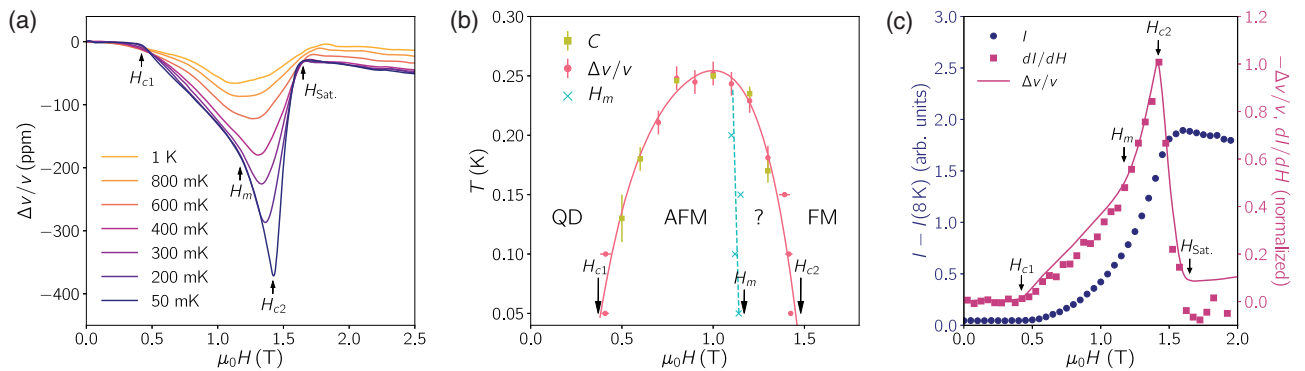


FIG. 3. (a) Ultrasound velocity with longitudinally polarized sound waves along the c^* axis. (b) H vs T phase diagram for $\text{Yb}_2\text{Si}_2\text{O}_7$ with the points on the phase boundary determined by ultrasound velocity (pink circles and blue crosses) and specific heat (yellow squares). The field was applied along the c axis (specific heat) and c^* axis (ultrasound). (c) Evolution of the (2,0,0) magnetic Bragg peak intensity (blue) versus field, $I(H)$, which is proportional to the square of the net magnetization. Additionally the derivative of the (2,0,0) magnetic Bragg peak intensity (square symbols) and the inverse of the ultrasound velocity data (solid line) are overlaid, showing agreement between these two measurements.

to coupling between the ultrasound velocity and antiferromagnetic fluctuations.

As the temperature is raised, the overall variations in sound velocity become much smaller in magnitude and the sharp features are smoothed out; hence we use temperature scans of sound velocity (see Supplemental Material [28]), which show small but fairly sharp anomalies, to establish the phase boundaries of the antiferromagnetic dome at higher temperatures. These boundaries are entirely consistent with the specific heat measurements.

The dome of field-induced order mapped out by the specific heat and ultrasound velocity data [Fig. 3(b)] is similar to the BEC phase of traditional QDMs, but there is an important difference: the dome in $\text{Yb}_2\text{Si}_2\text{O}_7$ is highly asymmetric, with an unusual regime in the high field part of the phase ($H > H_m$). Asymmetry of the dome can sometimes be attributed to quantum fluctuations in the proximity of H_{c1} , which is expected when $H_{c1}/(H_{c2}-H_{c1})$ is small. However, in $\text{Yb}_2\text{Si}_2\text{O}_7$ this number is 0.4, which is twice as large as the well-known case of dome asymmetry in DTN [43]. Further, this effect does not explain the high field phase above H_m . This unusual regime may be due to non-U(1) symmetric terms in the $S_{\text{eff}} = 1/2$ low energy effective Hamiltonian for $\text{Yb}_2\text{Si}_2\text{O}_7$. However, the strength of any anisotropic exchange is limited by our observation of a Goldstone-like mode (gapless to within $\delta E = 0.037$ meV) via INS, discussed below.

Figure 3(c) shows the field dependence of neutron diffraction (measured on FIE-TAX) at the (2,0,0) zone center. This reflection is only sensitive to the square of the net magnetization (m_z^2) that arises due to canting towards the field direction rather than any AFM components of the magnetic structure. The onset of magnetic order and growth of the net magnetization is confirmed above H_{c1} through the observation of increasing magnetic Bragg peak intensity. The intensity of the (2,0,0) peak shows an approximately quadratic increase, with a sudden change in the second derivative occurring at approximately H_m . Additionally, Fig. 3(c) shows a comparison of the first derivative of the (2,0,0) Bragg peak intensity at 50 mK and the negative of the relative ultrasound velocity at 100 mK, which are consistent (though this level of agreement is somewhat unexpected following a standard theoretical treatment, see Ref. [28]).

INS data provide evidence of the spontaneous breaking of an approximately continuous symmetry for fields between H_{c1} and H_{c2} . Figure 4 shows the INS spectra of $\text{Yb}_2\text{Si}_2\text{O}_7$ at $T = 50$ mK for representative applied fields along the c axis. In a QDM with Heisenberg exchange, the three excited dimer states are triply degenerate (forming a triplet with $S_{\text{tot}} = 1$, and $S_z = -1, 0$, and 1), and are then Zeeman split by the applied magnetic field. With finite interdimer exchange the resulting triplons are mobile, and the excited states become dispersive. For $\text{Yb}_2\text{Si}_2\text{O}_7$ below H_{c1} a resolution-limited single excited dispersive branch [bandwidth of 0.167(1) meV, and a gap

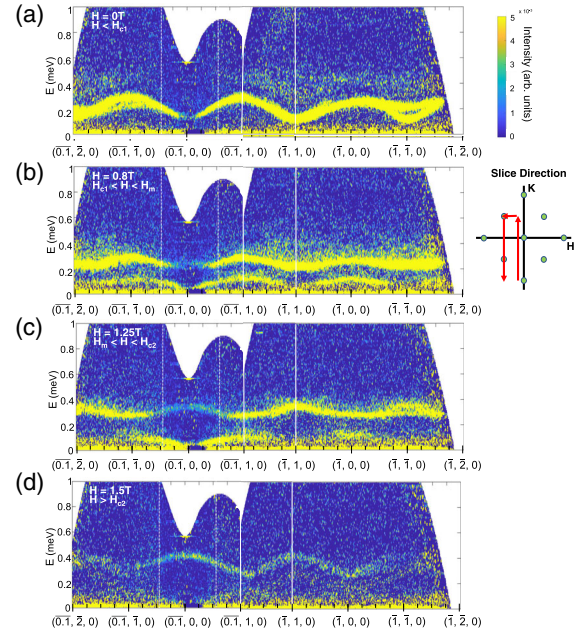


FIG. 4. INS data at $T = 50$ mK for four representative field strengths ($H \parallel c$). The path shown includes the reciprocal lattice directions $[-0.1K0]$, $[H10]$, and $[-1K0]$ as shown schematically to the right of the figure. All slices shown are integrated ± 0.1 r.l.u. in the perpendicular direction. At zero field [panel (a)], two bands are visible near $(\bar{1}, \bar{1}, 0)$ and $(\bar{0}, \bar{1}, \bar{1}, 0)$ due to a misaligned grain in the sample [28]. These are actually due to the same excitation which is identified as the $\psi_{1,0}$ state. Between H_{c1} and H_{c2} , a Goldstone mode appears, which is gapless at zone centers to within the energy resolution of the instrument, $\delta E = 0.037$ meV. Above H_{c2} the intensity of the excitation drops dramatically due to the system entering a field-polarized paramagnet state.

of 0.1162(4) meV] is visible. The apparent secondary branch observed around $(\bar{0}, \bar{1}, \bar{1}, 0)$ and $(\bar{1}, \bar{1}, 0)$ is due to a minority crystal grain. The energy of the observed excitation does not change for $H < H_{c1}$ as shown in the Supplemental Material [28], signifying that the angular momentum projection along the magnetic field is zero (i.e., $S_{\text{tot}} = 1$, $S_z = 0$, which we call $\psi_{1,0}$). The absence of apparent $S_{\text{tot}} = 1$, $S_z \pm 1$ modes (hereafter labeled as $\psi_{1,\pm 1}$) at most field strengths below H_{c1} indicates that the neutron scattering transition matrix elements from the ground state to $\psi_{1,\pm 1}$ are small compared to that for $\psi_{1,0}$. However, $\psi_{1,\pm 1}$ are discernible with very weak intensity at fields near H_{c1} indicating the transition matrix elements are nonzero [28]. Above H_{c1} , a new low energy excitation appears, which is gapless at the magnetic zone centers to within the energy resolution of the instrument ($\delta E = 0.037$ meV). This Goldstone mode implies spontaneous breaking of an approximate U(1) symmetry in the plane perpendicular to the applied magnetic field (the a^*-b plane), suggestive of the BEC transition observed in traditional QDMs [1,44]. Additionally, we note that the energy resolution is $\sim 16\%$

our estimated J_{intra} ; thus this measurement of the Goldstone mode actually allows for a potentially sizable anisotropic exchange contribution. Furthermore, the presence of a distinguishable region of the field-induced phase (between H_m and H_{c2}) is not expected for a simple Heisenberg or XXZ exchange. We find that in this field region the Goldstone mode persists, despite the lack of evidence for spontaneous symmetry breaking in $C_p(T)$ (i.e., a sharp anomaly is absent). However, the broad $C_p(T)$ feature does move to lower temperature as the field is further increased in this field region, tracing out the high-field side of the dome phase boundary. Above H_{c2} all of the excitations become fully gapped and the broad feature in C_p moves to higher temperature with increasing field, consistent with a field-polarized paramagnet. In the field-polarized regime, the inelastic intensity is greatly reduced due to the development of strong magnetic Bragg peaks at the elastic line, as expected based on the sum rule for magnetic neutron scattering.

Recently, rare-earth materials have been identified as potential hosts of Kitaev exchange in honeycomb materials [45]. In light of this, it is important to note that $\text{Yb}_2\text{Si}_2\text{O}_7$ is structurally similar to the famous Kitaev material Na_2IrO_3 [46], as they share the same space group and Wyckoff position of the magnetic species. Therefore, Kitaev exchange is allowed by symmetry in $\text{Yb}_2\text{Si}_2\text{O}_7$. If Kitaev exchange were dominant in $\text{Yb}_2\text{Si}_2\text{O}_7$ it could lead to a quantum spin liquid ground state [11]. Interestingly, the presence of a Goldstone mode does *not* rule out such anisotropic Kitaev exchange due to the “hidden” $\text{SU}(2)$ symmetries found within the extended Kitaev-Heisenberg model [47,48]. However, our fits to field polarized INS data are well-approximated by Heisenberg interactions, so Kitaev interactions are unlikely to be dominant in this material.

In summary, the strongly spin-orbit coupled material $\text{Yb}_2\text{Si}_2\text{O}_7$ realizes a QDM ground state with magnetic field-induced order reminiscent of a BEC phase. However, this ordered phase exhibits unusual characteristics at the high field part of the dome, including an abrupt change in the field dependence of the magnetization and sound velocity, and the loss of a sharp anomaly in the specific heat. The presence of a Goldstone mode throughout the full field-induced ordered state suggests dominant Heisenberg or XXZ exchange interactions, and the former is confirmed by fits to field polarized INS data and the zero field specific heat. However, the observation of the unusual regime between H_m and H_{c2} may imply that additional anisotropic interactions are necessary in order to fully describe the field induced phases of this novel quantum magnet. $\text{Yb}_2\text{Si}_2\text{O}_7$ provides the first example of a Yb^{3+} -based QDM with a possible field-induced BEC phase, adding this canonical example of quantum magnetism to the roster of quantum phases exhibited by materials based on this versatile ion.

This research was supported by the National Science Foundation Agreement No. DMR-1611217. J. Q.

acknowledges technical support from M. Castonguay and S. Fortier, informative conversations with G. Quirion, C. Bourbonnais, and I. Garate and funding from NSERC. The authors acknowledge the assistance of Aaron Glock and Antony Sikorski in the sample synthesis, as well as Craig Brown for his assistance with the BT1 neutron powder diffraction experiment. A portion of this work used resources at the Spallation Neutron Source and High Flux Isotope Reactor, which are DOE Office of Science User Facilities operated by Oak Ridge National Laboratory. The authors also acknowledge the support of the National Institute of Standards and Technology, U.S. Department of Commerce in providing some of the neutron research facilities used in this work.

*Gavin.Hester@colostate.edu

†Jeffrey.Quilliam@USherbrooke.ca

‡Kate.Ross@colostate.edu

- [1] V. Zapf, M. Jaime, and C. D. Batista, *Rev. Mod. Phys.* **86**, 563 (2014).
- [2] V. S. Zapf, D. Zocco, B. R. Hansen, M. Jaime, N. Harrison, C. D. Batista, M. Kenzelmann, C. Niedermayer, A. Lacerda, and A. Paduan-Filho, *Phys. Rev. Lett.* **96**, 077204 (2006).
- [3] M. Jaime, V. F. Correa, N. Harrison, C. D. Batista, N. Kawashima, Y. Kazuma, G. A. Jorge, R. Stern, I. Heinmaa, S. A. Zvyagin, Y. Sasago, and K. Uchinokura, *Phys. Rev. Lett.* **93**, 087203 (2004).
- [4] E. C. Samulon, Y. J. Jo, P. Sengupta, C. D. Batista, M. Jaime, L. Balicas, and I. R. Fisher, *Phys. Rev. B* **77**, 214441 (2008).
- [5] A. A. Aczel, Y. Kohama, C. Marcenat, F. Weickert, M. Jaime, O. E. Ayala-Valenzuela, R. D. McDonald, S. D. Selesnic, H. A. Dabkowska, and G. M. Luke, *Phys. Rev. Lett.* **103**, 207203 (2009).
- [6] A. A. Aczel, Y. Kohama, M. Jaime, K. Ninos, H. B. Chan, L. Balicas, H. A. Dabkowska, and G. M. Luke, *Phys. Rev. B* **79**, 100409(R) (2009).
- [7] M. Hermele, M. P. A. Fisher, and L. Balents, *Phys. Rev. B* **69**, 064404 (2004).
- [8] S. Onoda and Y. Tanaka, *Phys. Rev. Lett.* **105**, 047201 (2010).
- [9] K. A. Ross, L. Savary, B. D. Gaulin, and L. Balents, *Phys. Rev. X* **1**, 021002 (2011).
- [10] M. J. Gingras and P. A. McClarty, *Rep. Prog. Phys.* **77**, 056501 (2014).
- [11] A. Kitaev, *Ann. Phys. (Amsterdam)* **321**, 2 (2006).
- [12] G. Jackeli and G. Khaliullin, *Phys. Rev. Lett.* **102**, 017205 (2009).
- [13] J. G. Rau and M. J. P. Gingras, *Phys. Rev. B* **98**, 054408 (2018).
- [14] A. M. Hallas, J. P. Gaudet, N. P. Butch, M. Tachibana, R. S. Freitas, G. M. Luke, C. R. Wiebe, and B. D. Gaulin, *Phys. Rev. B* **93**, 100403(R) (2016).
- [15] L. S. Wu, W. J. Gannon, I. A. Zaliznyak, A. M. Tsvetlik, M. Brockmann, J.-S. Caux, M. S. Kim, Y. Qiu, J. R. D. Copley, G. Ehlers *et al.*, *Science* **352**, 1206 (2016).

- [16] L. S. Wu, S. E. Nikitin, Z. Wang, W. Zhu, C. D. Batista, A. M. Tsvelik, A. M. Samarakoon, D. A. Tennant, M. Brando, L. Vasylychko *et al.*, *Nat. Commun.* **10**, 1 (2019).
- [17] S. Ono, J. Despault, L. Calvert, and J. Taylor, *J. Less Common Metals* **22**, 51 (1970).
- [18] P. Gegenwart, H. Aoki, T. Cichorek, J. Custers, N. Harrison, M. Jaime, M. Lang, A. Ochiai, and F. Steglich, *Physica (Amsterdam)* **312B–313B**, 315 (2002).
- [19] J. G. Rau, L. S. Wu, A. F. May, L. Poudel, B. Winn, V. O. Garlea, A. Huq, P. Whitfield, A. E. Taylor, M. D. Lumsden *et al.*, *Phys. Rev. Lett.* **116**, 257204 (2016).
- [20] I. Kimchi, A. Nahum, and T. Senthil, *Phys. Rev. X* **8**, 031028 (2018).
- [21] A. Ochiai, T. Inukai, and T. Matsumura, *J. Phys. Soc. Jpn.* **76**, 123703 (2007).
- [22] Y. Kato, M. Kosaka, H. Nowatari, Y. Saiga, A. Yamada, T. Kobiyama, S. Katano, K. Ohoyama, H. Suzuki, N. Aso *et al.*, *J. Phys. Soc. Jpn.* **77**, 053701 (2008).
- [23] D. D. Khalyavin, D. T. Adroja, P. Manuel, A. Daoud-Aladine, M. Kosaka, K. Kondo, K. A. McEwen, J. H. Pixley, and Q. Si, *Phys. Rev. B* **87**, 220406(R) (2013).
- [24] Y. Nakanishi, F. Shichinomiya, M. Koseki, G. Koseki, R. Kashiwazaki, K. Deto, M. Nakamura, M. Yoshizawa, and M. Kosaka, *J. Phys. Conf. Ser.* **400**, 032062 (2012).
- [25] K. Hara, S. Matsuda, E. Matsuoka, K. Tanigaki, A. Ochiai, S. Nakamura, T. Nojima, and K. Katoh, *Phys. Rev. B* **85**, 144416 (2012).
- [26] S. Kittaka, T. Sugiyama, Y. Shimura, T. Sakakibara, S. Matsuda, and A. Ochiai, *J. Korean Phys. Soc.* **62**, 2088 (2013).
- [27] K. Momma and F. Izumi, *J. Appl. Crystallogr.* **44**, 1272 (2011).
- [28] See Supplemental Information at <http://link.aps.org/supplemental/10.1103/PhysRevLett.123.027201> for further details on: sample preparation, CEF considerations, specific heat fitting and high temperature data, ultrasound velocity measurements, INS data under different magnetic field strengths, fits to the field polarized INS data, magnetization data at 2K, and powder x-ray diffraction, which includes Refs. [29–36].
- [29] M. Rotter, D. Manh Le, J. Keller, L. G. Pascut, T. Hoffmann, M. Doerr, R. Schedler, P. Fabi, S. Rotter, M. Banks *et al.*, *McpPhase users manual: Symmetry considerations for crystal field parameters*, https://www2.cpfs.mpg.de/~rotter/homepage_mcpPhase/manual/manual.html.
- [30] A. Abragam and B. Bleaney, *Electron Paramagnetic Resonance of Transition Ions* (Oxford University Press, Oxford, 2012).
- [31] J. A. Quilliam, K. A. Ross, A. G. Del Maestro, M. J. P. Gingras, L. R. Corruccini, and J. B. Kycia, *Phys. Rev. Lett.* **99**, 097201 (2007).
- [32] Q. Gu and J. L. Shen, *Eur. Phys. J. B* **18**, 63 (2000).
- [33] M. Troyer, H. Tsunetsugu, and D. Würtz, *Phys. Rev. B* **50**, 13515 (1994).
- [34] G. Quirion, X. Han, and M. L. Plumer, *Phys. Rev. B* **84**, 014408 (2011).
- [35] S. Toth and B. Lake, *J. Phys. Condens. Matter* **27**, 166002 (2015).
- [36] J. Felsche, *J. Less-Common Met.* **21**, 1 (1970).
- [37] Y. I. Smolin and Y. F. Shepelev, *Acta Crystallogr. Sect. B* **26**, 484 (1970).
- [38] H. Nair, T. DeLazzer, T. Reeder, A. Sikorski, G. Hester, and K. Ross, *Crystals* **9**, 196 (2019).
- [39] G. Ehlers, A. A. Podlesnyak, J. L. Niedziela, E. B. Iverson, and P. E. Sokol, *Rev. Sci. Instrum.* **82**, 085108 (2011).
- [40] R. T. Azuah, L. R. Kneller, Y. Qiu, P. L. Tregenna-Piggott, C. M. Brown, J. R. Copley, and R. M. Dimeo, *J. Res. Natl. Inst. Stand. Technol.* **114**, 341 (2009).
- [41] Z. Wang, D. L. Quintero-Castro, S. Zherlitsyn, S. Yasin, Y. Skourski, A. T. M. N. Islam, B. Lake, J. Deisenhofer, and A. Loidl, *Phys. Rev. Lett.* **116**, 147201 (2016).
- [42] O. Chiatti, A. Sytcheva, J. Wosnitza, S. Zherlitsyn, A. A. Zvyagin, V. S. Zapf, M. Jaime, and A. Paduan-Filho, *Phys. Rev. B* **78**, 094406 (2008).
- [43] Y. Kohama, A. V. Sologubenko, N. R. Dilley, V. S. Zapf, M. Jaime, J. A. Mydosh, A. Paduan-Filho, K. A. Al-Hassanieh, P. Sengupta, S. Gangadharaiah, A. L. Chernyshev, and C. D. Batista Gangadharaiah, *Phys. Rev. Lett.* **106**, 037203 (2011).
- [44] T. Giamarchi, C. Rüegg, and O. Tchernyshyov, *Nat. Phys.* **4**, 198 (2008).
- [45] F.-Y. Li, Y.-D. Li, Y. Yu, A. Paramekanti, and G. Chen, *Phys. Rev. B* **95**, 085132 (2017).
- [46] S. Hwan Chun, J. W. Kim, J. Kim, H. Zheng, C. C. Stoumpos, C. D. Malliakas, J. F. Mitchell, K. Mehlawat, Y. Singh, Y. Choi *et al.*, *Nat. Phys.* **11**, 462 (2015).
- [47] J. Chaloupka, G. Jackeli, and G. Khaliullin, *Phys. Rev. Lett.* **110**, 097204 (2013).
- [48] J. Chaloupka and G. Khaliullin, *Phys. Rev. B* **92**, 024413 (2015).